

RSC Advances



This article can be cited before page numbers have been issued, to do this please use: S. Ghosh, S. S. Acharyya, M. Kumar and R. Bał, *RSC Adv.*, 2015, DOI: 10.1039/C5RA03803K.



This is an *Accepted Manuscript*, which has been through the Royal Society of Chemistry peer review process and has been accepted for publication.

Accepted Manuscripts are published online shortly after acceptance, before technical editing, formatting and proof reading. Using this free service, authors can make their results available to the community, in citable form, before we publish the edited article. This *Accepted Manuscript* will be replaced by the edited, formatted and paginated article as soon as this is available.

You can find more information about *Accepted Manuscripts* in the [Information for Authors](#).

Please note that technical editing may introduce minor changes to the text and/or graphics, which may alter content. The journal's standard [Terms & Conditions](#) and the [Ethical guidelines](#) still apply. In no event shall the Royal Society of Chemistry be held responsible for any errors or omissions in this *Accepted Manuscript* or any consequences arising from the use of any information it contains.

COMMUNICATION

One-pot preparation of nanocrystalline Ag/WO₃ catalyst for the selective oxidation of styrene

Cite this: DOI: 10.1039/x0xx00000x

Shilpi Ghosh,^a Shankha S. Acharyya,^a Malika Kumar^b and Rajaram Bal^{*a}Received 00th January 2012,
Accepted 00th January 2012

DOI: 10.1039/x0xx00000x

www.rsc.org/

Cationic surfactant cetyltrimethylammonium bromide-mediated water-based preparation of nanocrystalline Ag/WO₃ catalyst has been reported in a one-pot preparation method. This catalyst has been characterized by XRD, XPS, SEM, TEM, STEM-mapping, FTIR, Raman, TGA, and ICP-AES. SEM images displayed the formation of aloevera-like structure. TEM-images revealed the formation of ultrasmall Ag (with average size 5 nm), anchored on monoclinic WO₃ rods (with diameter in the range between 80 and 120 nm). It was found that the catalyst can effectively oxidize styrene with H₂O₂ as oxidant. The effect of different reaction parameters have been studied in detail. A styrene conversion of 75% with a styrene-oxide selectivity of 55% and a styrene conversion of >99% with a benzaldehyde selectivity of 88% accomplished over this catalyst, varying different reaction conditions. The catalyst did not show any leaching up to five reuses, showing the true heterogeneity of the catalyst. However, significant H₂O₂ decomposition occurs on the catalyst necessitating its usage in four-fold excess.

One-dimensional (1D) nanostructures (such as wires, rods, tubes, and belts) have been the focus of extensive research in recent years due to their potential applications in fabricating nanoscale electronic, optoelectronic, sensing devices and catalysis. More recently, many efforts have been devoted to the controlled synthesis and assembly of metal nanowires owing to their promising use as interconnects or active components in fabricating nano-devices and their important roles in probing a variety of physical phenomena.¹⁻³ Additionally, the surface of 1D nanomaterials is inherently rich in coordinatively unsaturated sites that can play an active role in catalytic reactions.⁴ Thus, 1D nanomaterials are drawing growing

attention for the specific physical properties that they display compared to their bulk counterparts. Solution-phase techniques (wet chemistry) have been shown to be a very advantageous and viable approach for the preparation of metal-oxide nanomaterials.⁴ However, these methods typically require the use of templates or other additives to direct the growth of the material towards a specific morphology. Cetyltrimethyl ammonium bromide (CTAB) is a cationic surfactant that plays an important role in controlling the formation of micro and nano architectures under the template effect (soft template). The growth of the certain architecture is associated with the selective interaction of the organic surfactants on certain crystallographic facets to stimulate the crystal growth.^{5,6}

Herein, we report a one-pot, CTAB-mediated, facile aqueous approach to prepare a forest of oriented silver-tungsten aloevera type material, that consists of numerous nanorods (1D) at room temperature. The morphology of the diameter and length of the nanorods in the system can be tuned by varying the experimental parameters. To the best of our knowledge, there is no literature present that reported the synthesis of this type of 1D composite nanomaterial previously.

Direct functionalization of hydrocarbons by catalytic oxidation of C-H bonds to form oxygenated products under mild conditions is a major challenge, since this path serve as the key to the formation of value-added oxygenated chemicals and pharmaceuticals.^{7,8} Among many oxidation reactions, catalytic oxidation of styrene is one of the most notable examples since the reaction gives valuable oxygenated compounds, which can serve as precursors for many chemical products like styrene oxide, acetophenone and benzaldehyde, and even benzoic acid.⁹ Among these oxygenates styrene oxide and benzaldehyde are the most important oxygenates. Styrene oxide, which is an important intermediate for large variety of fine

chemicals such as perfumes and drugs etc. Traditionally, oxidation of styrene is carried out by using stoichiometric amounts of organic peracids as oxidant.¹⁰ On the other hand, benzaldehyde (almond aroma) is the second most used flavouring agent.¹¹ In 2009, it was estimated that 90 kilotons of benzaldehyde were synthesized through industrial processes hampered by high temperatures and pressures that nevertheless resulted in lackluster yields.¹¹ One industrial pathway to benzaldehyde is the hydrolysis of benzalchloride synthesis which generates large quantities of HCl as a by-product.¹² The alternative, and more popular industry method of air-oxidation of toluene, results in low conversions of starting materials and produces benzaldehyde only as a by-product in the production of the less valuable benzoic acid.¹² But production of a specific oxygenate selectively, with high yield is a great challenge to the researchers; so, many researchers came forward to sort out the problem using various oxidants like TBHP,¹³⁻¹⁵ molecular oxygen,^{11,16,17} and a mixture of TBHP and molecular oxygen.¹⁸ In contrast to the said oxidants, use of H₂O₂-based catalytic epoxidation is of great advantage to the environment and industry because (i) it generates H₂O as a sole by-product, (ii) it has a high content of active oxygen species (47%), and (iii) H₂O₂ is rather inexpensive compared with organic peroxides and peracids¹⁹ and several researchers reported styrene-oxidation with H₂O₂ as oxidant. Laha et. al. demonstrated that, the yield of styrene oxide from styrene can be increased to ~52% if urea is mixed with H₂O₂ as oxidant, using TS-1 catalyst.²⁰ Rajabi et. al reported ~95 % yield of benzaldehyde from styrene using supported Fe-nanoparticles and H₂O₂ as oxidant.²¹ Duarte et. al. reported ~58% yield of benzaldehyde using tetrabutylammonium salt of [XW₁₁M(H₂O)O₃₉]^{(n-m)-}, X= B and M=Mn (III).²² But, so far and so forth, none of the process could have been scaled up largely because either low selectivity of styrene oxide/benzaldehyde, or use of high temperature, or serious leaching of the catalyst. In our previous paper, we reported ~ 52% yield of styrene oxide;²³ but the catalyst shows inefficiency from its 3rd recycle and suffers severe leaching in the reaction medium. Therefore, a true heterogeneous catalyst (devoid of leaching properties) with high selective nature is highly demanding in the field of catalysis. The heterogeneous epoxidation of olefins by silver-based catalysts is an important process in chemical technologies,^{16,24} and the catalytic properties of AgNPs in oxidation reactions strongly depend on the particles' size and stability and the nature of the support.

Herein, we also report a styrene conversion of 75% with a styrene-oxide selectivity of 65% and a styrene conversion of >99% with a benzaldehyde selectivity of 88%, varying reaction parameters.

The Ag/WO₃ aloevera catalyst was synthesized by modifying our own preparation method²⁵ taking tungstic acid and silver nitrate as the precursors of W and Ag respectively. The evolution of silver supported tungsten oxide aloevera-like structure is really interesting although the mechanism is not very clear. The cationic surfactant CTAB, synthesis- stirring time nucleation-growth rate of the seed plays an important role in determining the morphology of the final nanoparticle. As per LaMer plot²⁶ for the crystallization nucleation growth process and Tran's point, the nucleation rate increases with decreasing surface energy. The surfactant can affect surface energy and thus control the nucleation rate. According to Gibbs-Wulff theory, the equilibrium shape of a crystal is one that minimizes the surface energy for a given enclosed volume. If the surface energy is isotropic, the equilibrium shape will be spherical as the sphere has the minimum surface area. Inorganic nanoparticles often lead to spherical particles as this represents the lowest possible surface energy. 1D nanostructures is generated, if the surface energy is

anisotropic.²⁶ To explore the formation mechanism of Ag-WO₃ alovera, a series of time-dependent experiments were performed. In the absence of CTAB, disperse rods with indefinite aspect ratio were obtained (Fig. S1, ESI†). However, inhomogeneous rod-like nanostructures with small diameters assembled by disordered aspect ratio were obtained while Ag: CTAB molar ratio was 1: 1 (Fig. S2, ESI†). This experimental finding reflected the structure-directive property of CTAB. When the mixture was kept for 1h aging, followed by calcinations, the product so obtained displayed that numerous nanoparticles assembled together and in a definite direction, the growth of the assembly occurred (shown by red arrows, Fig. S3, ESI†). 3h aging time was proved to be optimum condition for the growth of the alovera-type morphology. The SEM image of the sample displayed that almost homogeneously formed nanorods (1D) with diameter ~ 70 nm grew in a definite direction and displayed alovera-like morphology (Fig. S4, ESI†). While the aging time was prolonged to 10 h, these nanorods fused together by means of Ostwald ripening process and produced larger, indefinite-shaped aggregates (Fig. S5, ESI†).

As a cationic surfactant, CTAB is an ionic compound that ionized completely in water: quantities of anions OH⁻, WO₄²⁻, and Ag and cations CTA⁺, Ag⁺ existed in basic solution.²⁷ Therefore, cooperative self-assembly between ionic CTAB molecules and charged species is built via electrostatic interaction in reaction solution. The formation of nearly spherical aggregates of nanoparticles after 3h aging time may be brought from the strong electrostatic attraction between positive CTA⁺ cations and negative OH⁻ anions on the surface of nanoparticles as well as the hydrophobic interactions and van der Waals attraction caused by adjacent CTAB adsorbing on Ag-WO₃ nanoparticles. All these factors contribute greatly for the generation of alovera-like morphology of the sample. We also observed that, without the use of AgNO₃, and even change in the precursors of Ag/W, however, alovera-type morphology was not generated. (Fig. S6-S8, ESI†). Therefore, we tentatively, suggest that, CTAB-micelles in the solution, precursors of Ag, W and even aging time directly take part in the shape-controlled synthesis of Ag/WO₃ alovera.

The Ag/WO₃ alovera like catalyst was characterized thoroughly by XRD, XPS, SEM, TEM, Raman, FTIR, TGA, BET surface area and ICP-AES. The crystal structure and phase purity of the Ag-W alovera-like catalyst were analysed by X-ray diffraction (XRD). The X-ray diffraction (XRD) pattern of the catalyst showed the peaks at 2θ values of 23.1°, 23.7°, 24.4°, 33.3° and 34.0°, confirm the formation of monoclinic WO₃ (JCPDS No. 43-1035, space group: P21/n) (Fig. 1). However, we could not observe any diffraction peaks assignable to metallic silver Ag (0) or oxides of silver, indicating the very small silver particles size. No other peak due to other phase of tungsten-oxide was observed, indicating a useful method to synthesize high-purity under the present experimental conditions. XPS was utilized to detect the surface composition and the chemical state of the catalyst. X-ray photoelectron spectroscopy (XPS) analyses confirmed the presence of metallic silver (Ag) in the fresh sample from the corresponding Ag 3d_{5/2} and Ag 3d_{3/2} binding energy values of 368.2 eV and 374.2 eV respectively (Fig. S9, ESI†).²⁸ The W 4f_{5/2} and 4f_{7/2} spectra attributed to the binding energies 37.9 eV and 35.8 eV respectively suggesting that the tungsten in the tungsten oxide sample exists as W⁺⁶ (Fig. S10, ESI†).²⁹ The corresponding Ag 3d binding energy of the spent catalyst ~368.2 eV, confirms that the oxidation state of metallic silver does not change during catalysis.

The topology of the catalyst was studied by scanning electron microscopy (SEM, Fig. 2 & S4, ESI†). SEM images with lower magnification (Figure 2a) revealed that the catalyst displays aloe-leaf-like structure. The oriented texture of the sample can be better seen from much lower magnification (Fig. S4, ESI†). A high magnification image of the catalyst (Fig. 2c) reveals that most of the nanorods are oriented and have a uniform diameter and length. It also seems from the diagram that Ag nano particles are visualized like water-droplets on aloe-leaf-leaves. SEM-EDX analysis (Fig. 2d) of the composite revealed that, there appears a distribution of Ag, W and O only, and no sort of C or Br. This observation indicated the complete removal of the structure-directing template (s). However, SEM-EDX analysis of the uncalcined composite revealed the presence of C and N as impurity (marked as blue circle, Fig. S11, ESI†). This experimental finding was further supported from TGA (Fig. 3) and FTIR analysis of the uncalcined catalyst (Fig. 4). TGA analyses (Fig. 3) were carried out to understand the various weight-loss regimes of the uncalcined catalyst. Three discrete regions of thermal decomposition can be observed; first weight-loss corresponds to the elimination of water followed by the decomposition of reactants to form NO_x and organic phases at 150 to 230 °C and finally the combustion process between 250° and 330 °C. A further mass loss is noticed between 350 and 450 °C due to the elimination of remaining carbon and organic compounds. This region is likely due to formation of a crystallized Ag-W-O inorganic phase. Further weight loss was not observed when the temperature was further increased from 480 to 600 °C, no weight loss speculated, indicating the formation of stable Ag/WO_3 catalyst in that temperature zone.

The embedment of CTAB molecules on the uncalcined catalyst was further confirmed from the FTIR analysis (Fig. 4). The peaks of the sample at 812, 1062 cm^{-1} can be assigned to the C-N^+ stretching modes of CTAB molecules.³⁰ The peak at 1378 and at 1462 cm^{-1} are assigned to symmetric mode of vibration of the head groups of the methylene moiety (N^+-CH_3) and CH_2 scissoring mode respectively.³⁰ The frequencies above 1600 cm^{-1} to 3000 cm^{-1} are due to CH_2 symmetric and antisymmetric vibrations, respectively. It is to be noted that, the shift of vibrations to lower frequency occurred as the alkyl chains experienced a more hydrophobic environment in Ag-W blocks upon the surface of which the CTA-moieties were supposed to be bound.² It can be inferred that, the mutual interactions between CTAB and the Ag-W surface have taken place. Some bands were detected at 2800–3020 cm^{-1} , which can be attributed to the CTAB surfactant. The FTIR spectrum of CTAB shows two intense bands at 2918 and 2846 cm^{-1} , corresponding to the asymmetric and symmetric stretching vibrations of C–CH in the methylene chains. The sharp bands at 1450–1500 cm^{-1} were specified as the deformation of $-\text{CH}_2-$ and $-\text{CH}$, and the weak band at 3011 cm^{-1} as the C– CH_3 asymmetric stretching and N–CH symmetric stretching vibrations of the solid surfactant.³⁰ These typical frequencies were absent when the material was calcined at 500 °C in air (fresh catalyst) in the case of the prepared catalyst, which indicated that, the embedded CTAB moieties have been completely removed from the catalyst surface during calcination. In the crystalline structure of WO_3 , W atoms are located in the centre of WO_6 octahedra with O at the vertices forming W–O–W connections.³¹ For such an arrangement, the IR active bands are fundamental vibrations of W=O, W–O and W–O–W. These can be stretching (ν) or in-plane bending vibrations (δ) and out-of-plane wagging (γ).³¹ The main WO_3 vibrations are found in the 1700–380 cm^{-1} IR region. All synthesis temperatures present characteristic peaks at 570, 800, 895, 964, 1045, 1404 and 1608 cm^{-1} associated with $\gamma(\text{W-O-W})$, $\nu(\text{W-O-W})$, $\nu(\text{W-O-W})$, $\nu(\text{W-O, W=O})$, $\delta(\text{W-OH})$,

$\nu(\text{OH})$ and $\delta(\text{OH})$ in W–OH respectively. The $-\text{OH}$ bands are associated with surface hydroxyl groups and weakly bound solvent, ethanol/water. A stronger broad band around 3350 cm^{-1} should appear from a W–OH mode if intercalation of H_2O had occurred.³¹ Moreover, there was no structural deformation in the spent catalyst, that was observed from FTIR analysis.

To further investigate the surface property and to detect subtle phase information of the composite, we conducted Raman-spectrum analysis (Fig. 5). Raman spectra of the Ag/WO_3 flower catalyst is characterized by well resolved sharp bands as shown. The two main intense peaks at 806 and 718 cm^{-1} , are typical Raman peaks of crystalline WO_3 , which correspond to the stretching and bending vibrations of the bridging tungsten and oxygen atoms. They are assigned to be the W–O stretching (ν), W–O bending (δ) and O–W–O deformation (γ) modes, respectively. Two peaks at 326 and 274 cm^{-1} are assigned to be the bending $\delta(\text{O-W-O})$ vibrations.³¹ Those below 200 cm^{-1} modes were attributed to the lattice vibrations.³¹ After the reaction, the Raman spectrum of the spent catalyst was unchanged, reflects the structural stability of the catalyst under the reaction condition.

TEM was used to further investigate the sizes and shapes of the catalyst (Fig. 6). From the TEM image, it could be concluded that this preparation method has successfully overcome the problem of agglomeration and appropriate dispersion to obtain nanorods with uniform size. TEM measurements were carried out to check the particle size and distribution of the silver nanoparticles (Fig. 6b, inset, based on Fig. 6b). Higher magnification of the catalyst revealed that the catalyst is composed of highly dispersed very small silver nanoparticles of ~2-5 nm on WO_3 support (Fig. 6a,b). The corresponding TEM histogram of Ag nanoparticles showed a very narrow particle size distribution with sizes between 2.5-6.5 nm (Fig. 6b, inset). The interplanar spacing of the lattice fringe distance of 0.38 nm indicates the [020] lattice spacing of WO_3 , which was clearly discriminated from of 0.23 nm corresponds to [111] plane of Ag (Fig. 6d).²⁵ Additionally, the SAED pattern (Figure 6c) also displayed a polycrystalline nature of the aloe-leaf structure, indicating that the AgW rods are randomly orientated. Furthermore, the TEM image of the spent catalyst showed that the topology and the silver particle size of the catalyst were hardly changed after five reuses (Fig. S12, ESI†). TEM-EDX pattern also showed the presence of Ag and W in the sample (Fig. S13, ESI†). Moreover, that the percentage of Ag and W remain intact after four reuses qualitatively is also visualized from the corresponding TEM-EDAX image of the spent catalyst (Fig. S14, ESI†). It was also visualized from TEM-images (Fig. S15, ESI†), that increment in Ag-loading led to the increase in Ag-particle size. Moreover, some agglomerations of Ag-particles were also observed from the TEM diagram.

Typically, the dispersion of Ag, W and O atoms in the catalyst was also analyzed by STEM-EDX mapping (Fig. 7). It indicated that each of Ag, W and O species was homogeneously dispersed.

The activities of Ag/WO_3 aloe-leaf (Ag-W^{aly}) catalyst in the oxidation of styrene in liquid phase by using H_2O_2 as oxidant have been summarized in Table 1. Main product was detected to be styrene oxide (SO). Main by-products were detected to be benzaldehyde (ϕ_{CHO}), phenylacetaldehyde ($\phi_{\text{CH}_2\text{CHO}}$) and very less amount of benzoic acid (ϕ_{COOH}). Oxidation of styrene was speculated to occur in a single pathway i.e solely in the side chain, attached with aromatic system and none in the aromatic ring. At room temperature (35 °C), the poor conversion of styrene conversion was noticed. At higher temperatures (>50° C) although conversion of

styrene increased, selectivity to phenylacetaldehyde was noticed to be sharply dropping due to the formation of mainly benzaldehyde (Fig. S16, ESI†). To maintain the higher selectivity of SO, we tried to carry out the reactions at moderate temperature (at 75 °C), where we also expected the satisfied conversion of styrene (75% conversion). Then we varied different reaction conditions to achieve higher yield of SO at 75 °C. When styrene: H₂O₂ molar ratio was low (say 1:1 or 1:2), we observed low conversion of styrene (Fig. S17, ESI†) probably due to inevitable decomposition of H₂O₂ at that temperature over the catalyst. Blank reaction was performed (entry 1, Table 1 & Fig. S18, ESI†) without any catalyst; conversion of styrene was very poor, reflecting the necessity of the catalyst in this oxidation reaction. We also observed that, increment in catalyst weight decreased the selectivity of acetophenone (Fig. S18, ESI†), probably due to increase of more active catalytic sites facilitated the attacking positions of styrene in its all possible sites. Maintaining all the optimum conditions, when the reaction was allowed to run for hours (Fig. S19, ESI†), we noticed that, although the conversion of styrene increased with time, but SO selectivity gradually went decreasing due to the formation benzaldehyde and other by-products.

Notably, commercial Ag₂O, WO₃, and even metallic Ag catalyst did not show any activity (entry 2-4, Table 1). Conventional catalyst prepared by impregnation method also showed negligible activity (entry 5, Table 1). The reason can be attributed to the comparatively smaller size of Ag (supported) nanoparticles catalyst possess comparatively high specific surface area which corresponds to higher dispersion of the catalyst that leads to the availability of more exposed surface active sites, where the catalytic reaction takes place. The open structure of the WO₃ nanorods allows easy access of the reactants which makes the catalytic process favorable. The poor catalytic activity of the impregnated catalyst may be attributed to their irregular shape and larger particles size which limits the accessibility of the catalyst towards the reacting substrates (Fig. S13).

We also noticed that, further increment in content of Ag to 5.8%, however, the catalytic efficiency decreased (entry 9, Table 1). This may be attributed to the slightly aggregation of the Ag-NPs on the surface of WO₃ nanorods, resulting in the decrease of the number of active sites on the sample of the catalyst.

The optimum reaction condition of the oxidative coupling reaction was applied on various substituted styrenes (Table 2). Epoxides were the main product; moreover, we noticed that, electron-donating group facilitates the epoxidation reaction, whereas electron-withdrawing group retards it. From this experimental finding, it can be concluded that, the mechanism follows a radical-formation mechanism pathway.

The H₂O₂ does not interact with styrene under normal conditions. H₂O₂ dissociation is believed to occur homogeneously over the The dissociation of H₂O₂ over Ag/WO₃ generates the peroxo tungsten species which behave as an electrophile in this reaction and the electrophilic oxygen attacks the electron dense C=C bond; thereby SO moiety is produced on the surface of the catalyst.³² Hampering the optimum condition, i.e. use of excess H₂O₂ or use of higher temperature led to the rupture of 3-membered epoxy-system (SO) and produces more stable product benzaldehyde.

The oxidant H₂O₂ was used in an excess amount (styrene: H₂O₂ = 1: 4 molar ratio). In general, H₂O₂ decomposes spontaneously over a catalytic surface. Hence, we used an excess of H₂O₂ so that the active oxygen species needed for the oxidation of the styrene could be available during the reaction. Significant H₂O₂ decomposition occurs on the catalyst necessitating its usage in three-fold excess.

Furthermore, we took the reaction mixture and performed permanganometric titrations to detect H₂O₂, but no H₂O₂ was discovered in the reaction mixture, indicating that the unreacted H₂O₂ molecules have been decomposed completely. We have plotted H₂O₂ consumption in terms of its efficiency % (E_o) in Table 1.

The efficiency of a heterogeneous catalyst is evaluated in terms of its recyclability and stability. The reusability of the Ag-WO₃ aloe vera catalyst was studied without any regeneration. After each run, the catalyst was filtered during hot condition and repeatedly washed with acetonitrile and acetone and dried overnight at 100 °C and used as such. We observed that the catalyst showed negligible change in its activity (entry 7, Table 1 & Fig. S20, ESI†). The amount of Ag and W present in the catalyst after 5 reuse was almost same as the fresh catalyst (estimated by ICP-AES) confirming the true heterogeneity of the catalyst. After 5 recycles, negligible amount of leaching of Ag and W was detected by ICP-AES (concentration of both metals were <2 ppb).

Conclusions

In summary, we have developed a surfactant-promoted simple preparation method to prepare Ag/WO₃ aloe vera like catalyst, comprising 2.5-6.5 nm Ag nanoparticles anchored on WO₃ rods with ~70 nm diameter, displaying high thermal stability and good catalytic activity for the single step conversion of styrene to styrene oxide/benzaldehyde using H₂O₂, exhibiting a styrene conversion of 75% with a styrene-oxide selectivity of 55% and a styrene conversion of >99% with a benzaldehyde selectivity of 88% varying different reaction conditions. The catalyst can be reused several times without any activity loss. The proposed method is also advantageous from the standpoint of low cost, environmental benignity and operational simplicity; furthermore, it can be applicable to large-scale reactions.

Acknowledgements

SG and SSA thank UGC and CSIR, New Delhi, India, for their respective fellowships. R.B. thanks CSIR, New Delhi, for financial support in the form of the 12 FYP Project (CSC- 0125, CSC- 0117). The Director, CSIR-IIP is acknowledged for his help and encouragement. The authors thank ASD Division, IIP for the analytical services. We gratefully acknowledge Ms. Nishita Lucas, CSIR-NCL, Pune (India), for performing Raman spectroscopy analyses.

Notes and references

^a Catalytic Conversion & Processes Division, CSIR-Indian Institute of Petroleum, Dehradun-248005, India.

^b M. Tech. Chemical Synthesis & Process Technologies (CSPT), Department of Chemistry, University of Delhi, New Delhi, India

† Footnotes should appear here. These might include comments relevant to but not central to the matter under discussion, limited experimental and spectral data, and crystallographic data.

Electronic Supplementary Information (ESI) available: catalyst preparation, catalyst-characterization techniques, SEM diagrams, XPS, effects of different reaction parameters on styrene oxidation etc. See DOI: 10.1039/c000000x/

- 1 C. L. Jiang, F. Wang, N. Q. Wu and X. G. Liu, *Adv. Mater.*, 2008, **20**, 4826-4829.
- 2 Y. Cui, Q. Wei, H. Park and C. M. Lieber, *Science*, 2001, **293**, 1289-1292.
- 3 C. L. Jiang, S. Ranjit, Z. Y. Duan, Y. L. Zhong, K. P. Loh, C. Zhang and X. G. Liu, *Nanoscale*, 2009, **1**, 391-394.
- 4 W. Lueangchaichaweng, N. R. Brooks, S. Fiorilli, E. Gobechiya, K. Lin, L. Li, S. Parres-Esclapez, E. Javon, S. Bals, G. V. Tendeloo, J. A. Martens, C. E. A. Kirschhock, P. A. Jacobs and P. P. Pescarmona, *Angew. Chem.*, 2014, **53**, 1585-1589.
- 5 L. Z. Wang, J. L. Zhang, F. Chen and M. Anpo, *J. Phys. Chem. C*, 2007, **111**, 13648-13651.
- 6 L. P. Zhu, W. D. Zhang, H. M. Xiao, Y. Yang and S. Y. Fu, *J. Phys. Chem. C*, 2008, **112**, 10073-10078.
- 7 K. Kamata, K. Yonehara, Y. Nakagawa, K. Uehara and N. Mizuno, *Nature Chem.*, 2010, **2**, 478-483.
- 8 C. Jia, T. Kitamura and T. Fujiwara, *Acc. Chem. Res.*, 2001, **34**, 633-639.
- 9 S. S. Acharyya, S. Ghosh, R. Tiwari, B. Sarkar, R. K. Singha, C. Pendum, T. Sasaki and R. Bal, *Green Chem.*, 2014, **16**, 2500-2508.
- 10 D. Swern, *Organic Peroxide*; Wiley Interscience: New York, 1971.
- 11 M. J. Rak, M. Lerro and A. Moores, *Chem. Commun.*, 2014, **50**, 12482-12485.
- 12 F. Brühne and E. Wright, *Ullmann's Encyclopedia of Industrial Chemistry*, Wiley-VCH Verlag GmbH & Co. KGaA, 2000, DOI: 10.1002/14356007.a03_463
- 13 J. Liu, F. Wang, S. Qi, Z. Gu and G. Wu, *New J. Chem.*, 2013, **37**, 769-774.
- 14 S. Das, A. Goswami, M. Hesar, J. F. Al-Sharab, E. K. Mikmeková, F. Maran and T. Asefa, *Small*, 2014, **10**, 1473-1478.
- 15 B. Singh and A. K. Sinha, *J. Mater. Chem. A*, 2014, **2**, 1930-1939.
- 16 X. Liu, A. Klust, R. J. Madix and C. M. Friend, *J. Phys. Chem. C*, 2007, **111**, 3675-3679.
- 17 A. Dhakshinamoorthy, A. Primo, P. Concepcion, M. Alvaro and H. Garcia, *Chem. Eur. J.*, 2013, **19**, 7547-7554.
- 18 S. Sharma, S. Sinha and S. Chand, *Ind. Eng. Chem. Res.*, 2012, **51**, 8806-8814.
- 19 K. Kamata, K. Yonehara, Y. Sumida, K. Yamaguchi, S. Hikichi, and N. Mizuno, *Science*, 2003, **300**, 964-966.
- 20 S. C. Laha and R. Kumar, *J. Catal.*, 2001, **204**, 64-70.
- 21 F. Rajabi, N. Karimi, M. R. Saidi, A. Primo, R. S. Varma, R. Luque, *Adv. Synth. Catal.*, 2012, **354**, 1707-1711.
- 22 T. A. G. Duarte, A. C. Estrada, M. M. Q. Simões, I. C. M. S. Santos, A. M. V. Cavaleiro, A. G. P. M. S. Neves and J. A. S. Cavaleiro, *Catal. Sci. Technol.*, 2015, **5**, 351-363.
- 23 B. Sarkar, R. K. Singha, R. Tiwari, S. Ghosh, S. S. Acharyya, C. Pendum, L. N. S. Konathala and R. Bal, *RSC Adv.*, 2014, **4**, 5453-5456.
- 24 J. G. Serafin, A. C. Liu and S. R. Seyedmonir, *J. Mol. Catal. A: Chem.*, 1998, **131**, 157-168.
- 25 (a) S. Ghosh, S. S. Acharyya and R. Bal, *J. Mater. Chem. A*, 2014, **2**, 15726-15733; (b) S. Ghosh, S. S. Acharyya, T. Sasaki and R. Bal, *Green Chem.*, 2015, DOI: 10.1039/C4GC02123A.
- 26 Z. Jiang, J. Xie, D. Jiang, X. Wei and M. Chen, *CrystEngComm*, 2013, **15**, 560-569.
- 27 C. L. Kuo and K. C. Hwang, *Langmuir*, 2012, **28**, 3722-3729.
- 28 D. C. Lim, I. Lopez-Salido and Y. D. Kim, *Surf. Sci.*, 2005, **598**, 96-103.
- 29 N. Wang, D. Wang, M. Li, J. Shi and C. Li, *Nanoscale*, 2014, **6**, 2061-2066.
- 30 S. S. Acharyya, S. Ghosh and R. Bal, *ACS Appl. Mater. Interfaces*, 2014, **6**, 14451-14459.
- 31 O. Yayapao, T. Thongtem, A. Phuruangrat and S. Thongtem, *J. Alloys Compd.*, 2011, **509**, 2294-2299.
- 32 R. A. Sheldon and J. A. Van Doorn, *J. Catal.* 1973, **31**, 427-437.

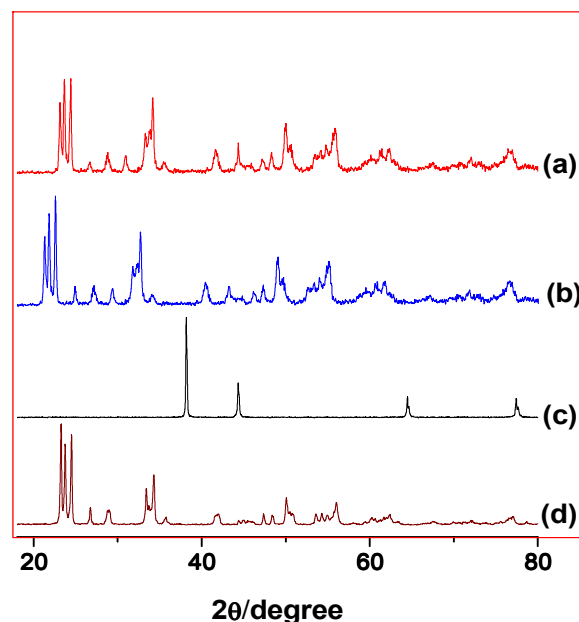


Fig. 1 XRD diffractogram of (a) fresh catalyst, (b) spent catalyst (after 4 recycles), commercial (c) Ag and (d) WO₃.

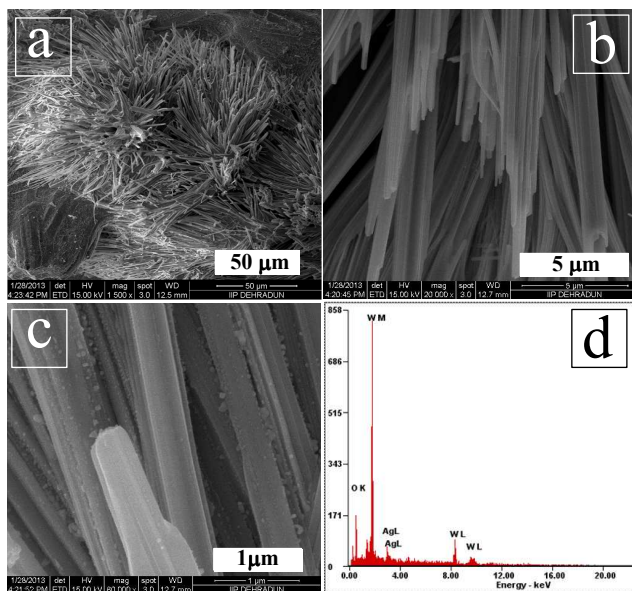


Fig. 2 SEM images (a-c) in increasing magnifications and (d) SEM-EDAX of Ag/WO₃ aloevera-type catalyst.

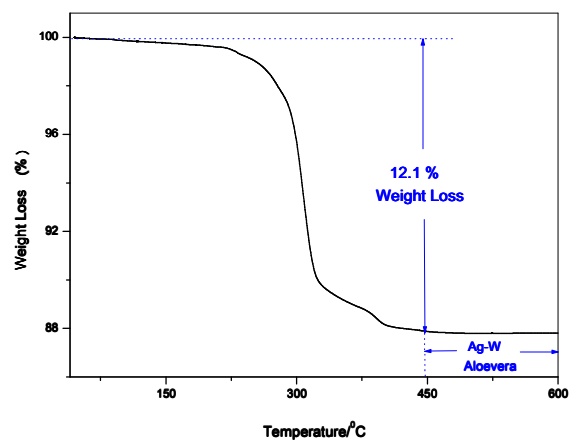


Fig. 3 TGA diagram of the uncalcined Ag/WO₃ aloevera-type catalyst.

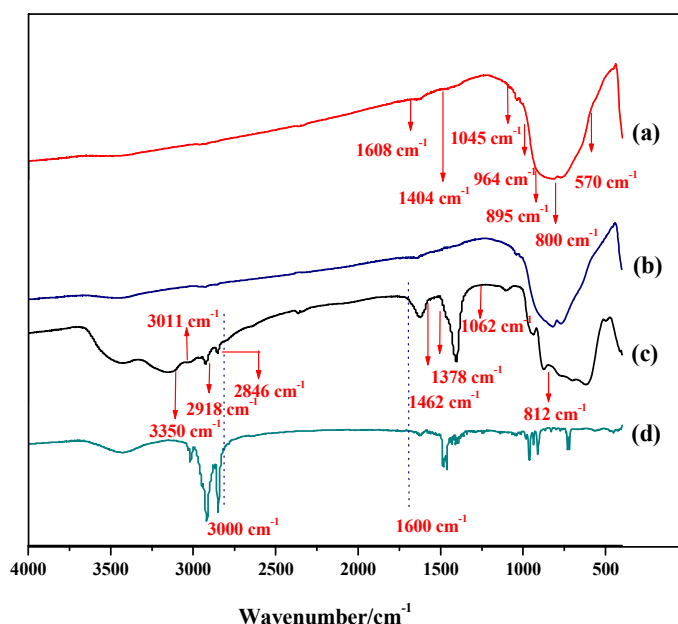


Fig. 4 FTIR diagram of (a) fresh and (b) spent (after 5 reuses), (c) uncalcined Ag/WO₃ aloevera-type catalyst and (d) that of CTAB.

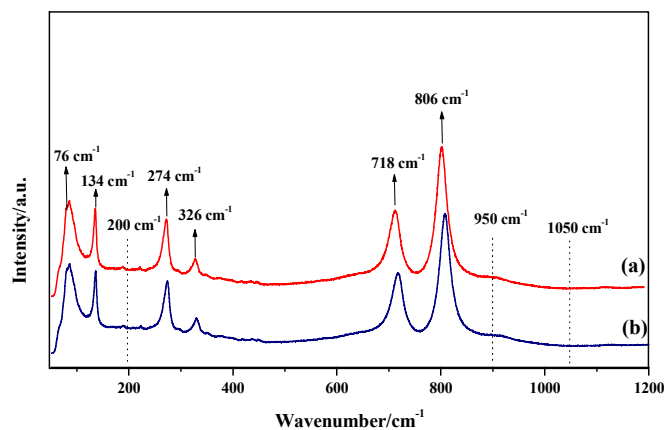


Fig. 5 Raman diagram of (a) fresh and (b) spent (after 5 reuses) Ag/WO₃ aloevera-type catalyst.

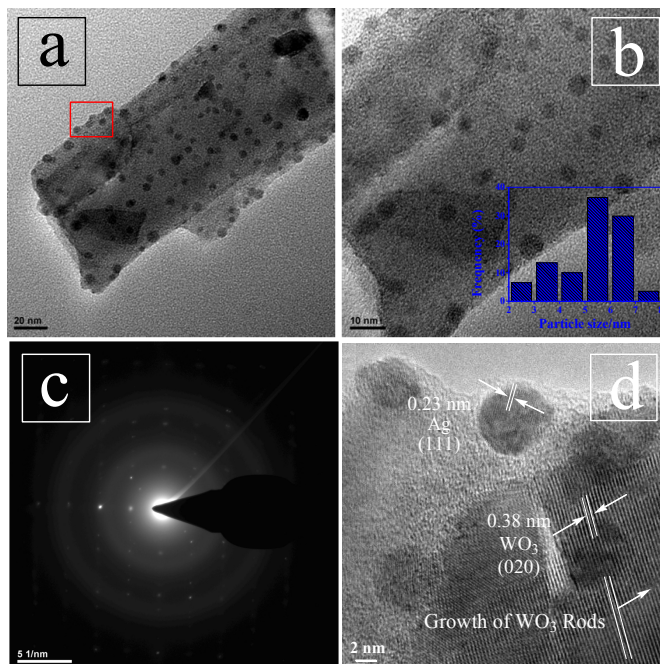


Fig. 6 TEM images (a, b) with increasing magnifications, (c) SAED pattern and (d) HRTEM image of the Ag/WO₃ aloevera-like catalyst.

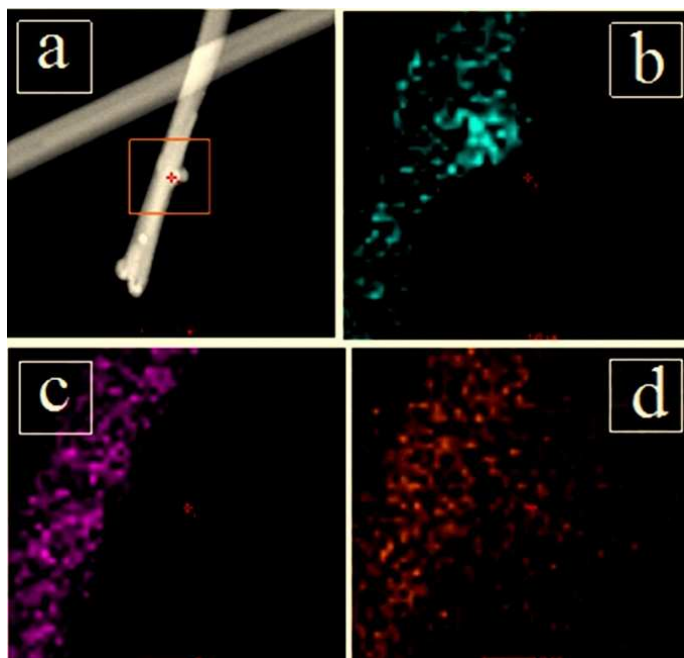


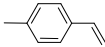
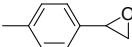
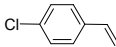
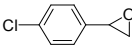
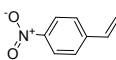
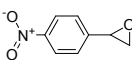
Fig. 7 (a) STEM image and elemental distribution (based on Figure 7a) of (b) Ag, (c) W and (d) O in the Ag-WO₃ aloevera-like catalyst.

Table 1. Oxidation Reaction of Styrene over Ag-W Aloe vera-like Catalyst^a

entry	catalyst	C _S ^b (%)	S _P ^c (%)				Y _{SO} ^d (%)	E ₀ ^e
			SO	ϕCHO	ϕCH ₂ C HO	ϕCOO H		
1	No catalyst	1.5	35	45	17	3	0.5	-
2	Ag	1.8	18	48	30.5	3.5	0.3	-
3	Ag ₂ O	2.2	14	46.5	35	4.5	0.3	-
4	WO ₃	2.8	22	52	20.5	5.5	0.6	-
5	Ag-W ^{imp}	2.5	26	56	15	3	0.6	-
6 ^f	Ag-W ^{alv3.3}	75	55	43	2	1	41.2	10.3
7 ^g	Ag-W ^{alv3.3}	72.5	52	44	2.5	1.5	37.7	9.4
8 ^h	Ag-W ^{alv3.3}	>99.0	5	88	3	4	5	14.5
9 ⁱ	Ag-W ^{alv5.8}	>99.0	27	67	3	2	1	16.5

^aTypical reaction conditions: solvent (MeCN) = 10 ml, substrate (styrene) = 1g, catalyst = 0.075 g, styrene: H₂O₂ (molar ratio) = 1:4, reaction temperature = 75 °C; time = 12 h; ^bC_B = Conversion of styrene based upon the FID-GC using methanol as external standard = [Moles of styrene reacted/initial moles of styrene used] x 100; ^cS_P = Selectivity to SO = [Moles of products produced/ moles of styrene reacted] x 100; ^dY_{SO} = Yield of SO = C_S x S_{SO}/100; ^eE₀ = H₂O₂ efficiency = [moles of SO or Benzaldehyde formed/total moles of H₂O₂ added] x 100. ^fPrepared Ag-WO₃ aloe vera catalyst and ^gcatalyst after 5 reuse; ^h styrene: H₂O₂ (molar ratio) = 1:6; ⁱAg loading = 5.8%; COM: commercial; IMP: impregnation method; alv: aloe vera-like; loading of Ag was determined from ICP-AES.

Table 2. Formation of SO's from Different Substituted Styrenes^a

entry	substrates	main product	C _S (%)	S _{SO} (%)	Y _{SO} (%)
1			78	48	37.4
2			55	37	20.3
3			18	27	4.9

^aTypical reaction conditions: solvent (MeCN) = 10ml, substrate = 1g, catalyst= 0.075g, substrate: H₂O₂ (molar ratio) = 1:4, reaction temperature = 75 °C; time = 12 h.